# The Photo-Stability of Polymer Solar Cells: Contact Photo-Degradation and the Benefits of Interfacial Layers

*Graeme Williams, Qi Wang, and Hany Aziz**

**The organic/electrode interfaces in organic solar cells are systematically studied for their light, heat, and electrical stability in an inert atmosphere. Various extraction layers are examined for their effect on device stability, including poly(3,4-ethylenedioxythiophene) poly(styrenesulfonate) (PEDOT:PSS) and $MoO_3$ for hole extraction layers, as well as LiF, $Cs_2CO_3$, and lithium acetylacetonate (Liacac) for electron extraction layers. The organic/metal interface is shown to be inherently photo-unstable, resulting in significant losses in device efficiency with irradiation. X-ray photoelectron spectroscopy measurements of the organic/aluminum interface suggest that the photo-induced changes are chemical in nature. In general, interfacial layers are shown to substantially reduce photo-degradation of the active layer/electrode interface. In spite of their photo-stability, several interfacial layers present at the active layer/cathode interface suffer from thermal degradation effects due to temperature increases under exposure to light. Electrical aging effects are proven to be negligible in comparison to other major modes of degradation.**

## 1. Introduction

Limited device stability remains one of the most significant roadblocks toward the wide success and commercialization of organic solar cells (OSCs). Gradual changes in the materials cause the power conversion efficiency of an OSC to decrease with time, thus limiting its useful (i.e., service) life. To this end, the vast majority of OSC stability research has focused on degradation due to ambient moisture and oxygen, which affects both the bulk active layer as well as the organic-electrode interface.[1–7] Ambient stability measurements provide very relevant information regarding degradation of the end-product solar cell. In addition, some efforts have been made to also understand the stability behavior of OSCs under illumination, even in an inert environment, referred to as device photo-stability.[8–11] In an inert atmosphere one may simply isolate the major pathways toward OSC photo-degradation: direct photo-induced changes, changes induced by associated thermal stresses, and changes induced by the flow of photo-generated charge carriers and/or their accumulation in trap sites in the various layers of a device, i.e., due to electrical stress.

We recently found that the organic layer/electrode interfaces in organic optoelectronic devices can degrade rapidly under illumination, even in inert environments.[12,13] Studies on organic light emitting devices (OLEDs) and organic photodetectors (OPDs) made of small molecule organic semiconductor materials reveal that photochemical changes at the metal and indium tin oxide (ITO) interfaces play a major role in limiting device stability.

In this work, we study the stability of polymer OSCs under illumination, focusing on the organic/electrode contacts and their influence on device photostability behavior. In particular, we use the archetypical OSC system based on a blend of poly(3-hexylthiophene) (P3HT) and [6,6]-phenyl-C61-butyric acid methyl ester (PCBM) active layer with ITO and aluminum electrodes, for hole and electron collection respectively. Since interfacial layers are often used at organic/electrode interfaces in OSCs, their influence on device stability is also investigated. Interfacial layers are generally used in OSCs to facilitate the extraction of the photogenerated charge carriers (holes and electrons) from the active layer to the corresponding hole- and electron-selective electrodes. Therefore, depending on their location in the device, these layers can be classified according to their functionality into (i) hole extraction layers (HELs), and (ii) electron extraction layers (EELs). Commonly used HEL and EEL materials include poly(3,4-ethylenedioxythiophene) poly(styrenesulfonate) (PEDOT:PSS)[14–16] and $MoO_3$[9,17] for HELs, and LiF,[8,18] $Cs_2CO_3$,[19,20] poly(ethylene glycol) (PEG),[6,7] $TiO_x$,[11,17,21] and ZnO[22,23] for EELs; the latter two materials are usually used in inverted solar cells, i.e., where the top electrode serves as the hole-extracting electrode. Since the studied devices were made in the more widely used upright architecture, we examined PEDOT:PSS and $MoO_3$ for HELs, and LiF and $Cs_2CO_3$ for EELs. We also studied a new EEL material, lithium acetylacetonate (Liacac), which we found can provide enhancements in device stability when compared to the ubiquitous LiF EEL. Our results demonstrate that the active layer/metal interface is inherently photo-unstable and limits the OSC photo-stability. The results also show that the use of EELs can substantially enhance photo-stability, but they may reduce the thermal stability. Further, $MoO_3$ HELs slightly bolster the device stability

G. Williams, Q. Wang, Prof. H. Aziz
Department of Electrical and Computer Engineering & Waterloo Institute for Nanotechnology
University of Waterloo, 200 University Avenue,
Waterloo, ON, N2L 3G1, Canada
E-mail: hany.aziz@ecemail.uwaterloo.ca

DOI: 10.1002/adfm.201202567

compared to PEDOT:PSS. Finally, electrical aging effects are found to be of minor concern when compared to other degradation mechanisms. The results accentuate the need for new HEL and EEL materials, and shed a new light on the reasons behind the higher stability of inverted cells.

## 2. Results and Discussion

### 2.1. Photo-Stability Tests on OSCs with PEDOT:PSS HELs and Various EELs

A group of P3HT:PCBM solar cells with a PEDOT:PSS HEL and various (or no) EELs was irradiated continuously by white light (100 mW/cm$^2$) over a period of 168 h in a $N_2$ atmosphere. In order to monitor changes in their performance as a result of the light stress, the photovoltaic characteristics of the OSCs were measured at fixed time intervals during this period. For comparison, a second group of samples, made of the same materials and structures, was kept in the dark (in a $N_2$ atmosphere) for the same period of time. This group was used to test for aging effects that may occur in the devices with time regardless of the irradiation. Furthermore, in order to distinguish between photo-induced changes and any changes that may be caused by thermal stresses arising from the exposure to light, we used a third group of samples that was kept in $N_2$ in the dark, but heated to a temperature of ≈40 °C, which is a few degrees above the measured temperature of the photo-irradiated samples (the first group). This allowed for thermal effects to be slightly more pronounced in the data set from the third group versus that in the first group. Therefore all solar cells were fabricated in triplicate: one group of samples for exposing to light stress (denoted "light stress"), a second group of samples to be kept in the dark (denoted "dark") and a third group of samples for exposing to thermal stress (denoted "heat stress"). The average solar cell parameters for these devices (prior to aging) are detailed in **Table 1**. In general, the power conversion efficiency (PCE) values were around 2% for devices with EELs and 1% for the control devices that did not have any EEL. The PCE improvement by inclusion of an EEL is due to an increase in all relevant solar cell parameters, including short circuit current ($J_{sc}$), open circuit voltage ($V_{oc}$) and fill factor (FF). Such PCEs are in line with the large body of published data for devices with these materials and architectures, indicating that our devices can be treated as good representatives of the majority of OSCs made with this material system by other research laboratories.[24]

**Table 1.** Summary of PEDOT:PSS HEL/variable EEL OSC device parameters before aging.

| Device Description | $J_{sc}$ [mA/cm$^2$] | $V_{oc}$ [mV] | FF [%] | PCE [%] | $R_{sh}$ [Ω cm$^2$] | $R_s$ [Ω cm$^2$] |
|---|---|---|---|---|---|---|
| No EEL (control) | 5.9 | 505 | 38 | 1.1 | 1700 | 31 |
| LiF | 6.5 | 623 | 46 | 1.9 | 3300 | 25 |
| Liacac | 7.2 | 626 | 50 | 2.3 | 3500 | 18 |
| No EEL (post-anneal) | 7.4 | 612 | 48 | 2.2 | 4200 | 19 |

The normalized PCE, FF, $V_{oc}$ and $J_{sc}$ values for these devices over the 168-h aging scheme are all shown in **Figure 1**, all normalized to the original values to facilitate cross-comparisons. Normalized series resistances ($R_s$) and shunt resistances ($R_{sh}$) during aging are provided in the Supporting Information. The original photovoltaic results (i.e., not normalized) are also provided in the Supporting Information. Note that each data point in Figure 1 and Table 1 (as well as **Figure 2** and **Table 2**, discussed later) represents the average value from four to six samples in each group. It is further noted that the data presented in this figure comprise only a small subset of a larger body of data collected over a period of 18 months and obtained from tests on twelve to fifteen solar cell samples from each group. This specific subset of data presented in this figure was obtained from samples fabricated and tested over a shorter period of time (6 months) to minimize experimental variation. Statistical averages from the larger body of data (i.e., 12–15 samples for each group) are shown in Supporting Information Figure S2 and Figure S3. Clearly, the data shown herein are representative of the results that have been observed throughout the full duration of this study.

As shown in Figure 1, the light stress leads to significant degradation in the performance of all devices, and the effect is more severe in the control devices without the EEL, which exhibit a decrease in PCE to 60% of their initial values after exposure to light for 168 h. This degradation is not substantially due to thermal effects, as devices exposed to heat stress alone (i.e., without the light) displayed a decrease in their PCE to only ≈85% of their initial value over the same period of time, despite the slightly higher temperature of the heat-stressed devices relative to that caused by the illumination of the light-stressed devices. In contrast, the OSCs employing LiF and Liacac EELs show substantially improved photo-stability compared to the control device. To this end, the LiF devices decreased to ≈75% of their original PCE values within 168 h of light stress, and the Liacac devices decreased to only ≈90% of their original PCE values. These results clearly show that the photo-stability of OSCs is limited by some photo-induced changes that occur at the active organic layer/Al electrode interface, and that EELs can have significant benefits to improving the photo-stability by minimizing this photo-induced degradation.

It is noteworthy to point out that $Cs_2CO_3$ was initially included in this investigation as a potential EEL. However, $Cs_2CO_3$-based devices generally exhibited much lower efficiencies (roughly 50–75% of that of LiF-based devices) and much poorer stabilities compared to other materials. As such, $Cs_2CO_3$ is only noted here as a rather poor EEL choice for standard configuration solar cells. It has, however, been demonstrated as a reasonable EEL in inverted geometries.[19,20]

While the LiF and Liacac EELs improve photo-stability, they are also found to somewhat limit the thermal stability. Considering the degradation of the LiF-based devices, as shown in Figure 1, the heat-stressed devices exhibit a nearly identical reduction in PCE as the light-stressed devices. This convincingly proves that the reduction in PCE for these devices mostly arises from thermal degradation. Although the large portion of degradation for LiF EEL devices appears to be purely due to thermal

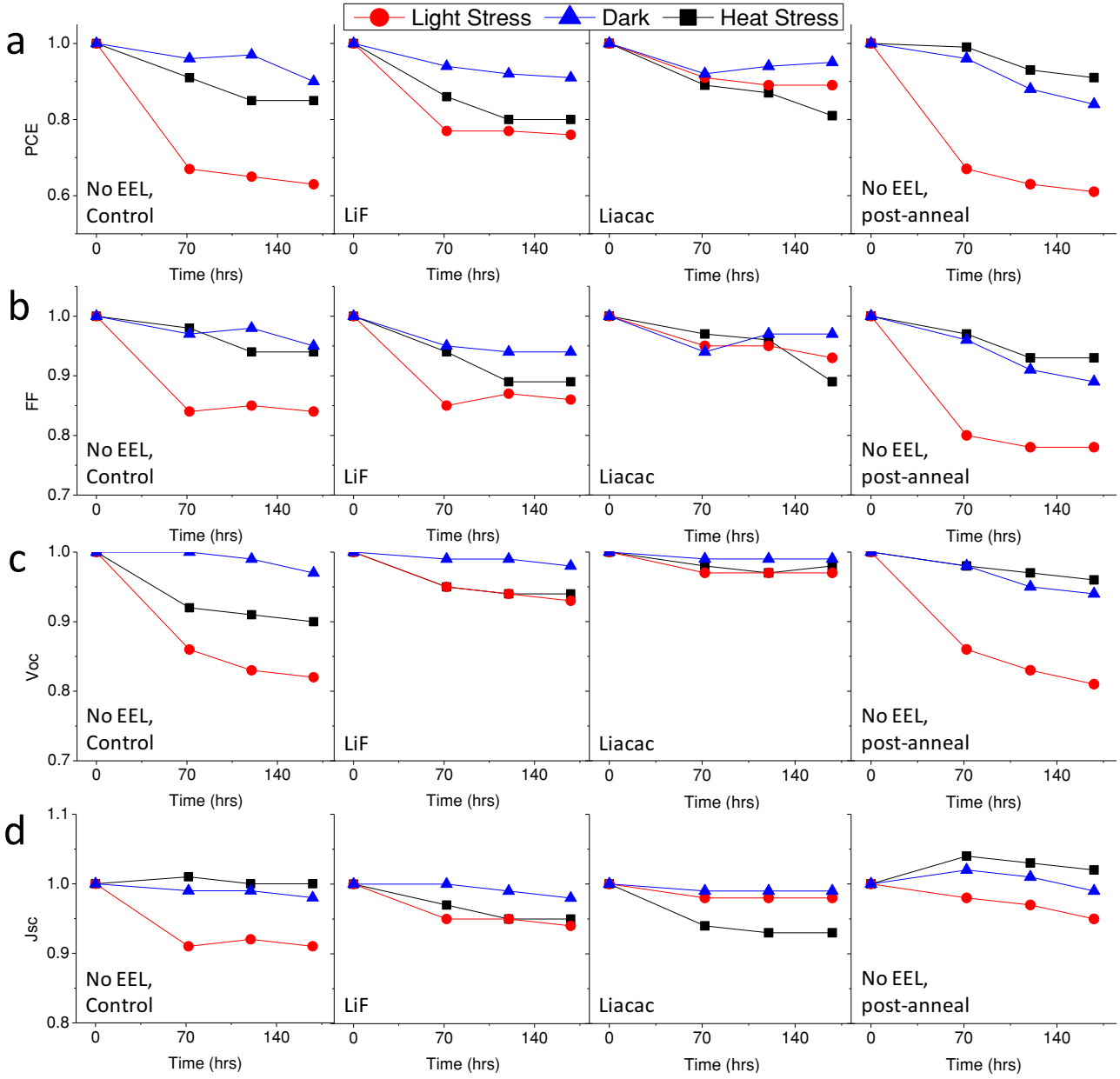


**Figure 1.** a) Normalized power conversion efficiency, b) fill factor, c) open circuit voltage, and d) short circuit current values of ITO/PEDOT:PSS/P3HT:PCBM/x/Al organic solar cells during 168-h aging studies. x = LiF, Liacac or nothing. (Note: all data points are taken as averages from 4–6 devices)

effects, the light-stressed devices have a slightly stronger reduction in PCE compared to the heat-stressed devices (decreasing to 75% vs 80% PCE). This difference is associated with a stronger reduction in fill factor for the light-stressed devices.

Finding that device photo-stability is governed by the active layer/Al interface, and that introducing an EEL at the interface can significantly improve OSC stability, it becomes interesting to see if altering the interface without using an EEL may have a similar effect. Therefore, we also studied devices where the annealing step in the device fabrication process was conducted after the Al metal electrode had been deposited (referred to here as "post-annealed") instead of the more common scenario where the annealing step is done prior to the metal deposition, as is also the case with the other devices in this study (commonly referred to as "pre-annealed"). The post-annealing process has been shown to drastically improve device parameters.[16,25,26] These improvements, especially the shift in $V_{oc}$ from 0.4 to 0.6 V, have been attributed to vertical segregation of the active layer, resulting in a more coherent interface with fewer shunt paths.[27] As detailed above and has been shown in literature,[18] a similar improvement in solar cell parameters can also be realized using pre-annealed devices in combination with an EEL, such as LiF. It is thus reasonable to conclude that the post-annealing step causes a change at the organic/Al interface,

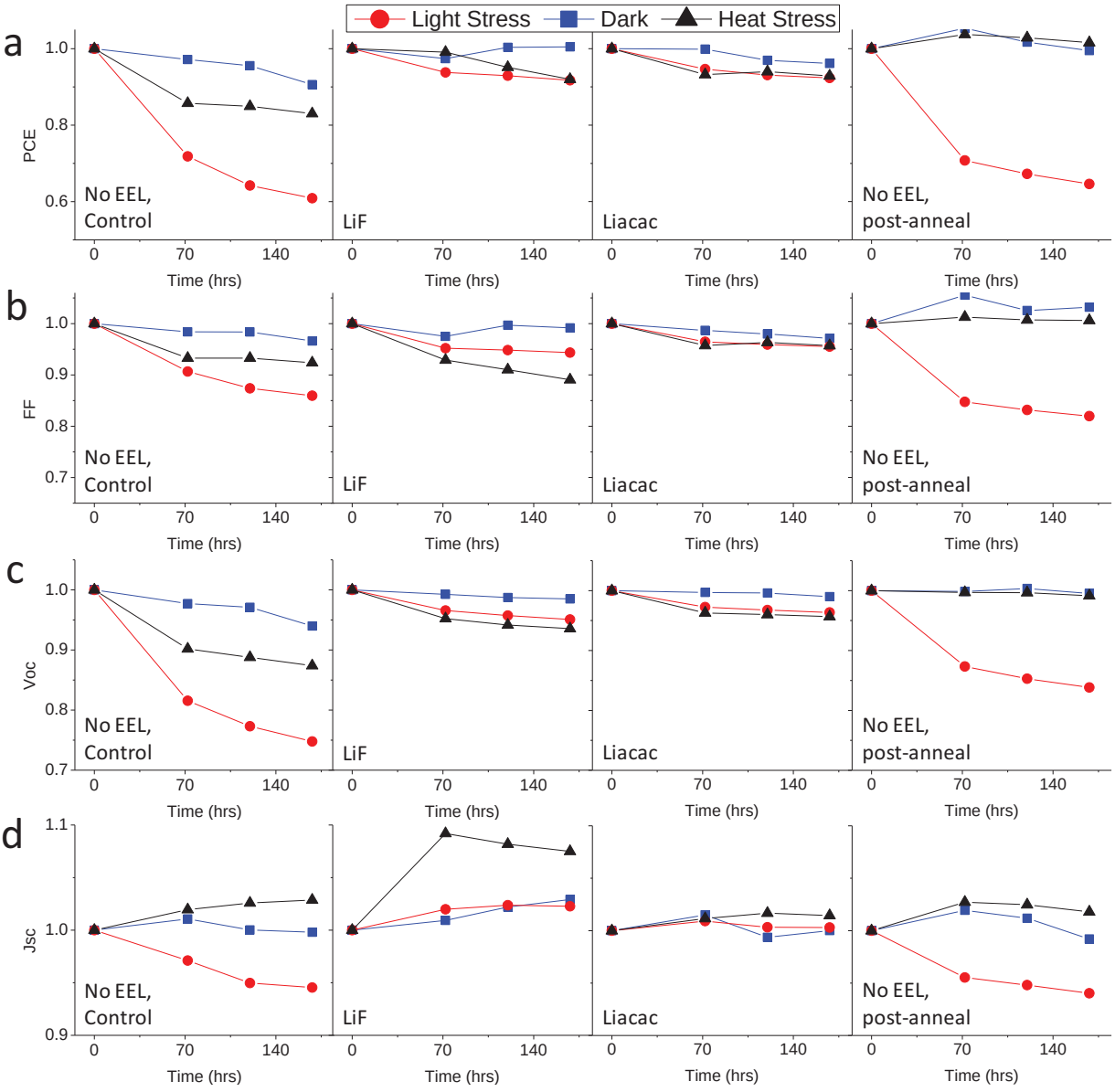


**Figure 2.** a) Normalized power conversion efficiency, b) fill factor, c) open circuit voltage, and d) short circuit current values of ITO/$MoO_3$/P3HT:PCBM/x/Al organic solar cells during 168-h aging studies. x = LiF, Liacac, or nothing. (note: all data points are taken as averages from 4-6 devices).

forming a quasi-EEL that helps improve electron extraction. As such, it becomes interesting to see if such devices may have different photo-stability behavior in comparison to the control (i.e., pre-annealed) devices.

The normalized PCE, FF, $V_{oc}$, and $J_{sc}$ values for the post-annealed devices over the 168-h aging scheme are also shown in Figure 1. Normalized $R_s$ and $R_{sh}$ values during aging are similarly provided in the Supporting Information. The average solar cell parameters for these devices (prior to aging) are also detailed in Table 1. As expected, annealing after Al deposition resulted in an improvement to all major solar cell parameters, allowing for a two-fold improvement in device PCE. The enhancement of FF was manifested as an increase in shunt resistance and a decrease in series resistance.

Quite interestingly, despite the performance improvement, the post-annealed devices have generally poor photo-stability, similar to that of the control devices, showing a decrease to 60% of the initial PCE within 168 h of light stress. As shown in Figure 1, this degradation is due to a deterioration in all relevant solar cell parameters (FF, $V_{oc}$ and $J_{sc}$), with the FF and $V_{oc}$ most strongly affected. The post-annealed sample experiences a slightly smaller reduction in $J_{sc}$ compared to the control sample, but this is compensated by a larger drop in FF. The post-annealed devices do, however, exhibit slightly enhanced thermal stability compared to the control devices. This variation is shown to be exclusively due to added stability in the $V_{oc}$, where the $V_{oc}$ of the heat-stressed post-annealed sample remained relatively constant. In contrast, the $V_{oc}$ of the heat-stressed control

**Table 2.** Summary of $MoO_3$ HEL/variable EEL OSC device parameters before aging.

| Device Description | Jsc [mA/cm$^2$] | Voc [mV] | FF [%] | PCE [%] | $R_{sh}$ [Ω cm$^2$] | $R_s$ [Ω cm$^2$] |
|---|---|---|---|---|---|---|
| No EEL (control) | 5.3 | 453 | 46 | 1.1 | 2600 | 21 |
| LiF | 5.3 | 622 | 56 | 1.8 | 3300 | 16 |
| Liacac | 5.7 | 621 | 56 | 2.0 | 3300 | 13 |
| No EEL (post-anneal) | 6.4 | 623 | 52 | 2.1 | 4500 | 18 |

sample decreased to ≈90% of its original value within the first 72 h. It is thus likely that this instability is due to heat-induced degradation at the organic/Al interface.

It is clear that in spite of the added thermal stability with post-annealing treatments, the active layer/Al interface is still very susceptible to photo-degradation. This suggests that simply altering the physical characteristics of the organic/Al interface, such as by annealing after the metal has been deposited, has little effect on the contact photo-stability, and that only changing the chemical nature of the interface, such as by introducing an inorganic EEL, may help increase OSC stability. It should also be noted that although in this study we only used Al as the top electrode material due to its very wide use in OSCs, interface photo-degradation is not specific to P3HT:PCBM/Al contacts, but rather occurs at the interfaces of various metals and organic materials,[13] suggesting that the phenomenon may be of a universal nature. To this end, it is suggested that the only requirements for photo-degradation are an organic/metal interface and the presence of photo-induced excitons.

### 2.2. Photo-Stability Tests on OSCs with $MoO_3$ HELs

Finding that the active layer/Al contact strongly influences OSC photo-stability it is natural to wonder if similar effects take place at the ITO contact. We therefore tested the effect of changing the HEL. $MoO_3$ is an attractive candidate, as it has recently been identified as a potential replacement to the traditional PEDOT:PSS HEL. To this end, work by Voroshazi et al. has identified an inter-electrode degradation mechanism (with ITO/PEDOT:PSS and Yb/Al contacts) possibly due to the moisture retained in PEDOT:PSS. These losses were shown to be suppressed by the use of a $MoO_3$ HEL instead.[9] Given that many EELs are essentially salts that may be strongly affected by the presence of moisture, it is desirable to extend the present analysis to P3HT:PCBM solar cells with a $MoO_3$ HEL. Comparing the parameters of OSCs with a $MoO_3$ vs a PEDOT:PSS HEL, the $MoO_3$ devices tended to have slightly lower $J_{sc}$ values that are compensated by corresponding increases with FF. Otherwise, the $V_{oc}$ and the PCEs of $MoO_3$ HEL devices were generally in the same range as PEDOT:PSS HEL devices. Note that the $MoO_3$ thickness can be varied from 0.5 to 15 nm with virtually no variation in OSC output parameters; for all of the devices detailed in this work, a thickness of 5 nm $MoO_3$ was used.

The normalized PCE, FF, $V_{oc}$ and $J_{sc}$ values for the $MoO_3$HEL devices over the 168-h aging scheme are shown in Figure 2, and the initial solar cell parameters (prior to aging) are shown in Table 2. Normalized $R_s$ and $R_{sh}$ values during aging are provided in the Supporting Information, along with the original photovoltaic (i.e., not normalized) results. The most noticeable difference between the stability of devices with PEDOT:PSS HELs versus those with a $MoO_3$ HEL is the near complete lack of degradation of the latter when kept in the dark. For the duration of this study, $MoO_3$ HEL devices that were kept in the dark retained 96% to 100% of their original PCE (with the exception of the control devices, i.e., without an EEL). The other major contrast when using $MoO_3$ is the behavior of $J_{sc}$ for the heat-stressed devices. For PEDOT:PSS HEL devices, $J_{sc}$ increased during the heat stress when no EEL was used, but decreased for LiF- and Liacac-EEL devices. For $MoO_3$ HEL devices, heat stress resulted in an increase to $J_{sc}$ by 2–10% for both the "No EEL" devices as well as those devices employing LiF and Liacac EELs. These differences can perhaps be explained by the presence of residual moisture in the PEDOT:PSS film. For degradation in the dark, residual moisture would ultimately degrade all solar cell parameters over time, analogous to OSCs that have been exposed to ambient moisture.[28] Further, heating may result in the gradual release of residual moisture from the PEDOT:PSS HEL, which could significantly affect the ultrathin LiF or Liacac EELs, considering their chemical nature as salts, and may cause them to release some species into the active layer of the OSC.[29] This could lead to the creation of recombination centres that would reduce $J_{sc}$, as observed for the PEDOT:PSS HEL devices. The contrasting increase in $J_{sc}$ for the $MoO_3$ HEL devices may be attributed to further improvement in the P3HT:PCBM layer morphology with heat, or due to a thermally induced change in the $MoO_3$ film. Further studies are currently underway to test these assertions.

The degradation behaviors of the $MoO_3$ HEL OSCs were otherwise very similar to the PEDOT:PSS devices. As shown in Figure 2, both the control and post-annealed "No EEL" devices showed substantial photo-degradation. The control device similarly showed heat stress degradation to $V_{oc}$ not observed in the post-annealed device. Introduction of an LiF or Liacac EEL substantially reduced direct photo-degradation, but the devices still suffered from thermal effects. This is shown for both the LiF and Liacac EEL devices, which have very similar final PCE values for the light-stressed and heat-stressed samples. As a point of note, the light-stressed and heat-stressed PCEs for both LiF and Liacac EEL devices were somewhat higher when making use of the $MoO_3$ HEL. More specifically, when employing an LiF or Liacac EEL, the $MoO_3$ HEL devices never dropped below 90% of the original PCE, whereas the PEDOT:PSS HEL devices ranged between 75% and 90%. The results therefore show that although using MoO3 instead of PEDOT:PSS as an HEL material can lead to some stability improvements, the benefits appear to be mostly due to lower moisture retention and/or improved thermal stability when using $MoO_3$ HEL, with no direct impact on photo-stability. These results can perhaps provide new sights on the reasons behind the general higher stability of inverted OSCs.[30] In this regard, the absence of the organic active layer/metal interface in inverted OSCs, which according to our findings appears to be strongly susceptible to photo-degradation and detrimental to the photo-stability, is perhaps one of the most important reasons. Furthermore, since $MoO_3$ is typically used instead of PEDOT:PSS as an HEL material in inverted

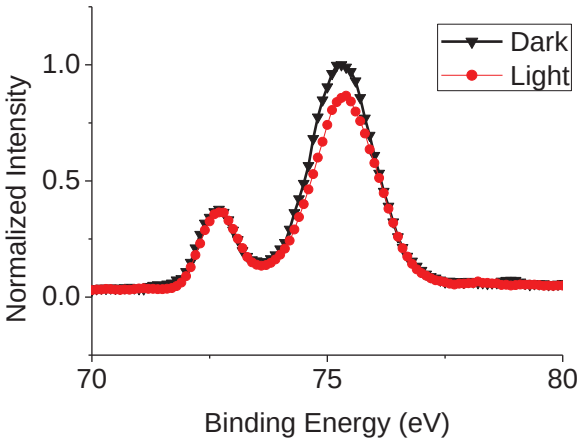


**Figure 3.** Al 2p binding energy spectra (by X-ray photoelectron spectroscopy) of P3HT:PCBM(70 nm)/Al(5 nm). Samples kept in dark and irradiated at 100 mW/cm$^2$ for 24 h.

cells, additional stability benefits can be expected, in light of our observations here.

### 2.3. X-Ray Photoelectron Spectroscopy Analysis of the Organic/Aluminum Interface

To gain some insight about the nature of the photo-induced changes at the active layer/metal interface, and whether the underlying processes are photochemical in nature, we used X-ray photoelectron spectroscopy (XPS) to probe changes in the chemical characteristics of the P3HT:PCBM/Al interface. The Al 2p binding energy spectra of P3HT:PCBM(70 nm)/Al(5 nm) samples are shown in **Figure 3**. In this figure, the "light" sample was irradiated with 100 mW/cm$^2$ white light from a halogen lamp for 24 h. Since both the light-stressed samples and the samples kept in the dark were fabricated on the same substrate (later cleaved for light aging and testing), the elemental aluminum peak at 72.7 eV has been normalized to the same intensity for both curves. A second peak is also observed at 75.3 ± 0.1 eV, which is shown to decrease significantly in intensity after irradiation. Note that aluminum oxide bonds form in this binding energy region, and some aluminum oxide is necessarily present due to the loading of the sample into the XPS chamber; however, a control/pure Al films on glass (without the P3HT:PCBM layer) showed negligible change in this region. It is thus suggested that the origin of this peak is due to Al–S by the thiophene component in P3HT[31,32] and/or Al–O–C by the carbonyl groups in PCBM (analogous to the peak observed in $Alq_3$[33]). The reduction of peak intensity post-irradiation suggests a decrease in bond density, indicating that the photo induced changes may indeed be chemical in nature. This implies that the active organic layer/aluminum interface is inherently susceptible to photo-degradation.

### 2.4. Electrical Aging Effects in Solar Cell Degradation

Although the above results clearly indicate that the major mode of degradation for the contacts interfaces is photo-induced, it is possible that the degradation is caused by the flow of electrical current (photo-generated carriers) through the OSCs, i.e., primarily due to electrical stress. Degradation due to charge accumulation and the associated electrical aging of organic layers has been identified as a significant mode of efficiency loss for OLEDs.[34] It is thus worth studying electrical stress effects in OSCs to ascertain their relative impact on device efficiency. To this end, electron-only and hole-only devices with the following structures were fabricated and studied:

- electron-only: ITO/Cs2CO3/P3HT:PCBM/(LiF, Liacac or No EEL)/Al
- hole-only: ITO/(PEDOT:PSS or $MoO_3$)/P3HT:PCBM/$MoO_3$/Ag

As both contacts in the first device are capable of injecting electrons efficiently into the P3HT:PCBM layer, but are much less efficient in injecting holes, the flow of current across the layers of the device under an external bias, regardless of the polarity, will occur predominantly through the transport of electrons, making it an "electron-only" device. Similarly, the hole-only device makes use of hole-injecting, but electron blocking, contacts allowing for only hole current with an applied bias.

The current density-voltage ($J$–$V$) characteristics of the devices are shown in **Figure 4**A and Figure 4B respectively. On these figures, a positive bias voltage corresponds to a bias where the ITO is at a more positive potential with respect to the Al. Considering the electron-only devices, the use of LiF or Liacac results in the highest level of injected current from the Al into the P3HT:PCBM layer, as shown in the positive bias region of Figure 4A. The LiF and Liacac EELs also exhibit very similar capacities to extract electrons from the P3HT:PCBM, as is evident from their similar current densities at any given voltage in the negative bias region of the $J$–$V$ curve. Further, both LiF and Liacac were more efficient in extracting electrons vs the No EEL control (note: in the negative bias region, electrons are injected into the P3HT:PCBM from the ITO/Cs2CO3 contact, and hence any differences in the current density at any voltage among the devices in this region reflects differences in the current extraction capacities at the Al electrode). The observations are in full agreement with the data in Tables 1 and 2 where the increase in PCE upon using the EELs is associated with a higher $V_{oc}$ and a lower $R_s$, both indicative of improved charge extraction and smaller $V_{oc}$ losses at the contact. The most efficient contact for extracting electron current, however, is the "No EEL" in the post-annealed sample, which is consistent with its high $J_{sc}$ noted in Table 1. For the hole-only devices, the ITO/$MoO_3$ contact is shown to have no observable Schottky barrier, providing slightly higher injected and extracted current compared to the PEDOT:PSS film. In general, the barriers to injection/extraction and the associated contact resistances were found to be much lower for the hole-only devices than for the electron-only devices.

In order to investigate possible degradation effects due to the prolonged flow of current, the electron-only and hole-only devices were subjected to a negative bias sufficient to maintain a continuous flow of current of –7.5 mA/cm$^2$ for 12 h in the dark, which is slightly higher than the highest short circuit current density observed with the OSCs subjected to the light stress tests in the first part of this study. A negative bias (hence

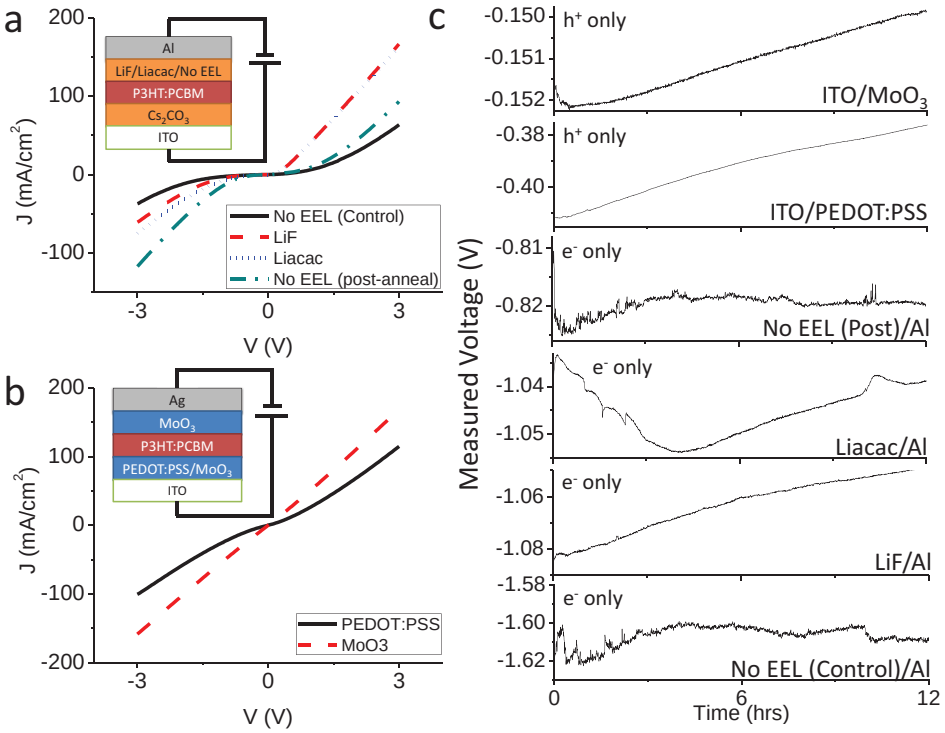


**Figure 4.** IV curves of a) electron- and b) hole-only devices. Insets: device structures and biasing scheme (note: negative bias = regular current flow during photovoltaic operation across interfaces of interest). c) Measured device voltages with –7.5 ma/cm$^2$ driving current over 12 h for various interfaces of interest.

the negative current density value) is used in order to make the flow direction of electrons and holes in these test devices the same as that of the photo-generated carriers in OSCs under normal conditions, i.e., electrons flowing from the P3HT:PCBM layer to the Al contact in case of the electron-only device, and holes flowing from the P3HT:PCBM layer to the ITO contact in the case of the hole-only device. The required voltages to maintain the –7.5 mA/cm$^2$ current density for the duration of these measurements are shown in Figure 4C. In general, the measured voltages remained relatively stable, varying only by 2 to 20 mV. Furthermore, subsequent current–voltage characteristic measurements after electrical stress showed insignificant variations from the original measurements–these data are not shown in Figure 4A,B, as the curves essentially overlap. These results indicate that electrical stress effects are relatively limited in OSCs, at least in the time frame of our experiment, and cannot account for the fast degradation in OSC performance observed with illumination.

The conclusion that the electrical stresses are insignificant is further supported by observations made during light-stress tests, where the OSCs were placed under both open circuit and short circuit conditions. In general, in the open circuit scenario, photogenerated charge carriers can be expected to exist in the active layer of the device when under illumination, but as the electrodes are electrically isolated and hence cannot dissipate charges collected from the active layer, the photogenerated charges will remain largely immobile. In contrast, in the short circuit scenario, the photogenerated charges will be able to flow through the organic layers, and across the various interfaces, to the electrodes then unto the external circuit. As such, should electrical stresses be significant, we would expect some differences in the rate of PCE decrease between these electrically different scenarios. Our results, however, showed that devices aged in both conditions gave very similar trends. Therefore, we have shown that the photo-induced changes in the previously examined OSCs are not due to the photo-induced flow of current or as a consequence of electrical stresses. Given these results, it is suggested that electrical stresses pale in comparison to other degradation mechanisms, such as light-, heat- and ambient $H_2O/O_2$-induced losses.

## 3. Conclusions

We have studied the stability behavior of P3HT:PCBM OSCs under illumination. Results show that exposure to light results in degradation in all OSC parameters, including their power conversion efficiency, even in inert environments. The degradation is found to be primarily due to photo-induced changes at the active layer/Al contact. XPS measurements suggest that these changes are photochemical in nature. The use of EELs in between the organic layer and the Al can largely suppress contact photo-degradation and enhance OSC photo-stability. In this regard, Liacac is proposed here as a new EEL material that is shown to provide efficiency improvements on par with the ubiquitous LiF, but with some additional stability improvements.

Using $MoO_3$ instead of PEDOT:PSS as an HEL material can result in stability improvements, likely due to the lower moisture retention and/or improved thermal stability. The results uncover a major degradation mechanism that limits OSC stability under illumination, and accentuate the need for new HEL and EEL materials. They also shed a new light on the reasons behind the higher stability of inverted cells.

## 4. Experimental Section

*Materials and Methods*: Reagent grade chemicals were purchased from Sigma Aldrich unless otherwise noted. Patterned ITO slides (6–8 Ω/□) were purchased from Luminescence Technology Corporation. PCBM (>99% pure) was purchased from 1-Material, ChemSciTech Inc. P3HT (>90% regioregular) was purchased from Rieke Metals, Inc through Sigma Aldrich. Any evaporated materials were thermally evaporated with the IntlVac OLED Thermal Evaporator using resistive boats under high vacuum (always below $5 \times 10^{-6}$ Torr) at rates of 1–5 Å/s, with the exception of $MoO_3$, which was evaporated at very low rates (<0.1 Å/s). Deposition rates were monitored using gold-coated quartz crystal sensors, which were calibrated to accurately determine film thicknesses with a Veeco Dektak 8 Stylus Profiler.

Preparation of the 1:1 ratio of P3HT:PCBM chlorobenzene solutions at 20 mg/mL solids was as follows: PCBM (20 mg/mL) was first prepared in chlorobenzene and placed on a hotplate at 62 °C and stirred at 650 rpm for 2 h. P3HT (20 mg/mL) was then prepared in chlorobenzene and added to the hotplate, with the temperature reduced to 57 °C while stirred at 650 rpm for 3 h. The PCBM solution was then mixed into the P3HT solution, and the P3HT:PCBM solution was stirred at 57 °C and 650 rpm for at least 1 h. The solution was removed from the hot plate and allowed to cool for approximately 15 to 30 min prior to use. Solutions were always used within the day of being prepared.

To fabricate the devices, patterned ITO slides were first cleaned by successive sonication in acetone, Micro-90 surfactant and isopropyl alcohol. The slides were scrubbed with a cotton swab after the acetone and Micro-90 sonication steps. The slides were then placed in an oven at 100 °C for at least one h but no longer than one day before use. Prior to deposition of interfacial or active layers, the slides were exposed to $O_2$ plasma using a Trion Phantom II RIE system equipped with an inductively coupled plasma source for 3 min. PEDOT:PSS layers were applied by spincoating Clevios P VP Al4083 PEDOT:PSS at 2300 rpm, followed by annealing at 180 °C for 10 min, to produce a 30-nm-thick film. LiF (1 nm), Liacac (0.5 nm), $Cs_2CO_3$ (0.5–2 nm) and $MoO_3$ (5 nm), as well as the 100 nm Al or Ag top electrode, were deposited via thermal evaporation using the methods noted above. For electron-only devices, ultrathin (≈0.5 nm) $Cs_2CO_3$ for was applied by spincoating a dilute solution of $Cs_2CO_3$ (0.1 wt%) in 2-ethoxyethanol at 4000 rpm and subsequently annealing at 150 °C for 20 min. The 70-nm active P3HT:PCBM layer was formed by spincoating at a spin speed of 1100 rpm for 60 s. This active layer film was then annealed at 110 °C for 10 min prior to the deposition of the top interfacial layer and the top electrode. In the case of post-annealed devices, the top Al electrode was deposited, and the device was subsequently annealed at 110 °C for 10 min. The device areas are defined by the overlap of ITO bottom electrode and Al top electrode to give devices that are 0.2 $cm^2$.

*Stability Tests*: Light-stress tests were carried out with white light provided by a 300 W halogen lamp. The distance between the lamp and the device was adjusted so that the light intensity was 100 $mW/cm^2$. Heat-stress tests were accomplished by covering the device with black electrical tape mask and putting it under another 300 W halogen lamp. The temperatures of the "light" and "heat" samples were monitored with a k-type thermocouple and an Omega panel monitor. Electrical stress tests were accomplished by driving a constant current of 7.5 $mA/cm^2$ and measuring the corresponding device voltage using an Agilent 4155C semiconductor parameter analyzer. All devices were kept in an inert nitrogen atmosphere at all times. Ambient moisture- and oxygen-related degradation effects are thus expected to be null and were specifically not included in this study.

*Measurements*: Photovoltaic parameters were measured with 1-sun AM1.5G radiation from an ABET Sun 3000 Class AAA Solar Simulator and a Keithley 2400 SourceMeter. Each patterned ITO slide allowed for 4–6 duplicates. As such, every measurement presented in this work is an averaged value from the duplicates. For the electrical stress tests, *J–V* measurements were performed with the Agilent 4155C semiconductor parameter analyzer. XPS was performed using a Thermo-VG Scientific ESCALab 250 Microprobe with a monochromatic Al KR source (1486.6 eV), capable of an energy resolution of 0.4–0.5 eV full width at half-maximum.

## Supporting Information

Supporting Information is available from the Wiley Online Library or from the author.

## Acknowledgements

Financial support to this work from the Natural Sciences and Engineering Research Council of Canada (NSERC) is gratefully acknowledged. GW also acknowledges financial support through NSERC Alexander Graham Bell Canada Graduate Scholarship, Ontario Graduate Scholarship, and Waterloo Institute for Nanotechnology Nanofellowship.

Received: September 6, 2012
Revised: November 2, 2012
Published online: December 10, 2012

[1] N. Grossiord, J. M. Kroon, R. Andriessen, P. W. M. Blom, *Org. Electron.* **2011**, *13*, 432.
[2] M. Hermenau, M. Riede, K. Leo, S. A. Gevorgyan, F. C. Krebs, K. Norrman, *Sol. Energy Mater. Sol. Cells* **2011**, *95*, 1268.
[3] M. Wang, F. Xie, J. Du, Q. Tang, S. Zheng, Q. Miao, J. Chen, N. Zhao, J. Xu, *Sol. Energy Mater. Sol. Cells* **2011**, *95*, 3303.
[4] M. Jorgensen, K. Norrman, F. C. Krebs, *Sol. Energy Mater. Sol. Cells* **2008**, *92*, 686.
[5] B. Paci, A. Generosi, V. R. Albertini, P. Perfetti, R. de Bettignies, J. Leroy, M. Firon, C. Sentein, *Appl. Phys. Lett.* **2006**, *89*, 043507.
[6] F. C. Chen, S. C. Chien, *J. Mater. Chem.* **2009**, *19*, 6865.
[7] S. C. Chien, F. C. Chen, M. K. Chung, C. S. Hsu, *J. Phys. Chem. C* **2011**, *116*, 1354.
[8] M. O. Reese, A. J. Morfa, M. S. White, N. Kopidakis, S. E. Shaheen, G. Rumbles, D. S. Ginley, *Sol. Energy Mater. Sol. Cells* **2008**, *92*, 746.
[9] E. Voroshazi, B. Verreet, T. Aernouts, P. Heremans, *Sol. Energy Mater. Sol. Cells* **2011**, *95*, 1303.
[10] S. Schäfer, A. Petersen, T. A. Wagner, R. Kniprath, D. Lingenfelser, A. Zen, T. Kirchartz, B. Zimmermann, U. Würfel, X. Feng, *Phys. Rev. B* **2011**, *83*, 165311.
[11] A. Hayakawa, O. Yoshikawa, T. Fujieda, K. Uehara, S. Yoshikawa, *Appl. Phys. Lett.* **2007**, *90*, 163517.
[12] Q. Wang, G. Williams, H. Aziz, *Org. Electron.* **2012**, *13*, 2075.
[13] Q. Wang, G. Williams, H. Aziz, *J. Appl. Phys.* **2012**, *112*, 064502.
[14] M. Reyes-Reyes, K. Kim, D. L. Carroll, *Appl. Phys. Lett.* **2005**, *87*, 083506.
[15] G. Li, V. Shrotriya, J. S. Huang, Y. Yao, T. Moriarty, K. Emery, Y. Yang, *Nat. Mater.* **2005**, *4*, 864.
[16] W. L. Ma, C. Y. Yang, X. Gong, K. Lee, A. J. Heeger, *Adv. Funct. Mater.* **2005**, *15*, 1617.
[17] C. Tao, S. P. Ruan, X. D. Zhang, G. H. Xie, L. Shen, X. Z. Kong, W. Dong, C. X. Liu, W. Y. Chen, *Appl. Phys. Lett.* **2008**, *93*, 193307.

[18] M. O. Reese, M. S. White, G. Rumbles, D. S. Ginley, S. E. Shaheen, *Appl. Phys. Lett.* **2008**, *92*, 053307.
[19] H. H. Liao, L. M. Chen, Z. Xu, G. Li, Y. Yang, *Appl. Phys. Lett.* **2008**, *92*, 173303.
[20] G. Li, C. W. Chu, V. Shrotriya, J. Huang, Y. Yang, *Appl. Phys. Lett.* **2006**, *88*, 253503.
[21] S. J. Yoon, J. H. Park, H. K. Lee, O. O. Park, *Appl. Phys. Lett.* **2008**, *92*, 143504.
[22] N. Sekine, C. H. Chou, W. L. Kwan, Y. Yang, *Org. Electron.* **2009**, *10*, 1473.
[23] M. S. White, D. C. Olson, S. E. Shaheen, N. Kopidakis, D. S. Ginley, *Appl. Phys. Lett.* **2006**, *89*, 143517.
[24] M. T. Dang, L. Hirsch, G. Wantz, *Adv. Mater.* **2011**, *23*, 3597.
[25] Y. Kim, S. A. Choulis, J. Nelson, D. D. C. Bradley, S. Cook, J. R. Durrant, *Appl. Phys. Lett.* **2005**, *86*, 063503.
[26] G. Li, V. Shrotriya, Y. Yao, Y. Yang, *J. Appl. Phys.* **2005**, *98*, 043704.
[27] H. Kim, W. W. So, S. J. Moon, *Sol. Energy Mater. Sol. Cells* **2007**, *91*, 581.
[28] K. Norrman, S. A. Gevorgyan, F. C. Krebs, *ACS Appl. Mater. Interfaces* **2009**, *1*, 102.
[29] Q. Wang, H. Aziz, *Org. Electron.* **2011**, *12*, 1571.
[30] F. Zhang, X. Xu, W. Tang, J. Zhang, Z. Zhuo, J. Wang, Z. Xu, Y. Wang, *Sol. Energy Mater. Sol. Cells* **2011**, *95*, 1785.
[31] P. Dannetun, M. Boman, S. Stafström, W. Salaneck, R. Lazzaroni, C. Fredriksson, J. Brédas, R. Zamboni, C. Taliani, *J Chem. Phys.* **1993**, *99*, 664.
[32] R. Lazzaroni, J. L. Bredas, P. Dannetun, M. Logdlund, K. Uvdal, W. R. Salaneck, *Synth. Met.* **1991**, *43*, 3323.
[33] M. G. Mason, C. W. Tang, L. S. Hung, P. Raychaudhuri, J. Madathil, D. J. Giesen, L. Yan, Q. T. Le, Y. Gao, S. T. Lee, L. S. Liao, L. F. Cheng, W. R. Salaneck, D. A. dos Santos, J. L. Bredas, *J. Appl. Phys.* **2001**, *89*, 2756.
[34] D. Y. Kondakov, J. R. Sandifer, C. W. Tang, R. H. Young, *J. Appl. Phys.* **2003**, *93*, 1108.